Research Article

Received: 14 January 2013 Revised: 11 April 2013 Accepted article published: 22 May 2013 Published online in Wiley Online Library: 11 July 2013

(wileyonlinelibrary.com) DOI 10.1002/pi.4563

Experimental characterization and computational simulations of the low-velocity impact behaviour of polypropylene

Juan P Torres,[a] Patricia M Frontini[a]* and Laurentzi Aretxabaleta[b]

Abstract

The objective of this work is to validate predictive models for the simulation of the mechanical response of polypropylene undergoing impact situations. The transferability of material parameters deduced from a particular loading scenario (uniaxial loading) to a different loading situation (multiaxial loading) was studied. The material was modelled with a modified viscoplastic phenomenological model based on the G'Sell–Jonas equation. To perform the numerical simulations, a user-material subroutine (VUMAT) was implemented in the ABAQUS/explicit finite element code. Constitutive parameters for the model were determined from isostrain rate uniaxial tensile impact test data using an inverse calibration technique. In addition, falling-weight low-energy impact tests were performed on disc-shaped specimens at velocities in the range 0.7 to 3.13 m s^{-1}. The model predictions were evaluated by comparison of the experimental and finite element response of the falling-weight impact tests. The G'Sell–Jonas model showed much better predictability than classical elastoplasticity models. It also showed excellent agreement with experimental curves, provided stress-whitening damage observed experimentally was accounted for in the model using an element failure criterion.

Keywords: polypropylene; low-energy impact; finite element method; constitutive modelling

INTRODUCTION

In the past few decades, there has been a continuously growing presence of thermoplastic polymers in highly demanding engineering fields such as the aeronautic, automotive, electronics and biomedical fields. In addition, there is particular interest in accurately predicting how such polymeric components will perform under high-impact conditions in safety-critical applications such as car crashes, accidental dropping, ballistic and blast loading.[1] Currently, when designing plastic parts or components for eventual or accidental impact, a series of expensive experimental trial-and-error tests on actual prototypes have to be carried out. This represents a costly routine, both in time and money. An alternative route, under constant development, is the prediction of the response of a material undergoing impact situations by means of computer simulations using finite element analysis (FEA). Two important features have to be taken into account when performing FEA simulations of polymeric materials: (i) the experimental method used to assess the intrinsic material behaviour aiming to calibrate the constitutive parameters and (ii) the constitutive model used to describe the true stress–strain relationship (due to its complex strain-rate, pressure and temperature dependency).

To obtain a correct description of the mechanical properties of polymers, the true stress–strain relationship needs to be measured experimentally. Also, it is desirable that these experimental curves are obtained at constant strain rate so that the constitutive dependence of the polymer with the deformation rate can be established. There are a number of experimental methods to evaluate the impact response of polymers: on the one hand, there are the traditional falling dart, Charpy, Izod and Gardner tests, which are only suitable for ranking polymers in terms of their impact performance since they impose inhomogeneous stress–strain fields and variable strain rates; on the other hand, there are the more recent split Hopkinson pressure bar (SHPB) and tensile impact tests, which have been used[1–3] for high strain rate (10^2–10^3 s^{-1}) testing. Although these novel methods are attractive for mechanical characterization, since the specimen is assumed to undergo homogeneous deformation, in both SHPB and tensile impact tests a constant strain rate cannot be achieved. To overcome this drawback, Aretxabaleta and co-workers developed a novel characterization method which involves the construction of isostrain rate curves from a series of tensile impact curves obtained at different impactor velocities.[3,4]

* *Corresponding to: Patricia M. Frontini, Instituto Nacional de Tecnología y Ciencia de Materiales INTEMA, Universidad Nacional de Mar del Plata, CONICET, Av. J. B. Justo 4302, B7608FDQ, Mar del Plata, Argentina. E-mail: pmfronti@fi.mdp.edu.ar*

a *Instituto Nacional de Tecnología y Ciencia de Materiales INTEMA, Universidad Nacional de Mar del Plata, CONICET, Av. J. B. Justo 4302, B7608FDQ, Mar del Plata, Argentina*

b *Department of Mechanical Engineering, Mondragon Goi Skola Politeknikoa, Mondragon Uniberstsitatea, Loramend 4, 20500 Mondragon, Spain*

Constitutive modelling of polymeric materials has received considerable attention during the past four decades. G'Sell and Jonas[5] derived a constitutive model that was used to approximate the flow curves of poly(vinyl chloride), and later high-density polyethylene and polypropylene.[6] They employed several temperatures, and strain rates ranging from 10^{-4} to 10^{-1} s^{-1}. Their model was also used to perform the simulation of stretching instabilities in polypropylene in pseudo-uniaxial tension which predicted accurately the evolution of specimen profile and engineering stress–strain curves. The G'Sell–Jonas model is a phenomenological model, in the sense that it was developed to fit intrinsic true stress *versus* true strain tensile curves, but was not derived from actual physical or molecular micromechanisms. Duan *et al.*[7] extended the G'Sell–Jonas model to a more complex model, the DSGZ model, intended to be more accurate in describing the entire range of deformation behaviour of both amorphous and semicrystalline polymers. In later investigations,[1] they used this model to simulate the impact of an amorphous acrylonitrile–butadiene–styrene polymer and semicrystalline poly(butylene terephthalate) polymer. For the calibration of their nine-parameter model, they used experimental data from uniaxial compression tests at low strain rates (10^{-3}–10^{-2} s^{-1}) together with SHPB for high strain rates (nominal 10^{3} s^{-1}). Their simulations showed good agreement with experimental data up to the maximum load. Billon *et al.*[8] validated the application of the G'Sell–Jonas constitutive model to a semicrystaline polymer, polyamide 12, for a large range of strain rates (up to 0.5 s^{-1}) during uniaxial tensile tests. However, they showed that the set of parameters determined during the tensile tests at low strain rates did not describe the behaviour of the same material during an impact test. Finally, they concluded that it seems impossible to characterize a polymer over a large range of strain rates and loading conditions using a set of constant coefficients. Following this reasoning, Viana *et al.*[9] employed an inverse analysis approach to obtain the parameters from experimental falling weight curves to assess the intrinsic high-strain-rate properties of their material. Using this method, they found good agreement between the computed and experimental curves. Nevertheless, it must be taken into account that for a constitutive model to be of practical utility in finite element modelling (FEM)-assisted design, it should reliably be capable of predicting behaviour outside of the conditions under which the parameters were determined. In the present investigation, the capability of the G'Sell–Jonas phenomenological model for predicting the impact response of a semicrystalline polymer, polypropylene, was evaluated by innovatively calibrating the constitutive parameters from tensile impact isostrain rate curves at high strain rates and comparing FEM predictions and experimental results under a different loading situation (in multiaxial falling weight tests).

Finally, it is important to mention that there has also been a series of physically inspired constitutive models which are derived by combining theories of macromolecular physics with recent work in the fields of statistical mechanics, continuum mechanics and computational mechanics. These models employ a constitutive framework intended to be general enough to capture material behaviour over a wide range of loading conditions in order to be appropriate for their use in FEM analysis. Among the most important contributions using this constitutive approach is the family of tri-dimensional models started by Boyce and co-workers,[10,11] with one of its latest additions focusing on the high strain rate response of amorphous polymers.[2] These models have been shown to be very accurate in modelling multiaxial stress states and inhomogeneous deformation fields. However, their mathematical formulation is not straightforward and their implementation as model subroutines to work in commercial FEM packages is very complex. Moreover, in most cases they require ten or more constants, to be determined using several experimental situations. For this reason, in this study this approach will not be employed.

EXPERIMENTAL

Tensile impact data

In tensile impact tests, a sample is fixed between a mobile grip and a fixed grip. A pendulum is released from a predetermined height and hits the mobile grip when it reaches its lowest point. Consequently, a tensile force is transmitted to the sample. This force is measured by a piezoelectric sensor at the fixed grip. The stress and strain fields generated can be supposed to be homogeneous in the calibrated part of the sample, unless necking appears. For the present work, experimental tensile impact isostrain rate curves obtained from an experimental programme developed previously[3,4] were used. In these investigations, injection-grade isotactic polypropylene homopolymer (SM6100K, Montell) was used. Tensile impact samples were cut from square plates of 1 mm nominal thickness obtained by injection moulding. The injected plates were annealed at 130 °C for 2.5 h to reduce internal stresses and orientation effects. Sample geometry and dimensions are shown in Fig. 1.

The generation of isostrain rate curves was performed as follows. First, force–time tensile impact curves were obtained for different velocities. Then, displacement–time curves were calculated by integrating the acceleration twice in time (the acceleration is simplified to be the force divided by the mass of the impactor). The strain was calculated as a function of displacement and the initial length of the samples:

$$\varepsilon(t) = \ln\left(1 + \frac{x(t)}{l_0}\right) \tag{1}$$

where $\varepsilon(t)$ is the logarithmic strain and $x(t)$ the displacement. Here a homogeneous deformation state along the test sample has been assumed following the assumptions of Aretxabaleta *et al.*[3] This approximation has been considered valid up to the breaking point since occurrence of a significant necking phenomenon was not observed (Fig. 10). Following, from the ε–t curves, $\dot{\varepsilon}(t)$ can be calculated by direct numerical derivation. Finally, σ–t curves are calculated from the force and strain data using

$$\sigma(t) = \frac{F(t)}{S_0}[1 + \varepsilon(t)] \tag{2}$$

where $F(t)$ is the uniaxial force, $\sigma(t)$ is the uniaxial stress and S_0 is the initial cross-section. Once $\dot{\varepsilon}$ –t curves are obtained, it remains to establish the strain rates to be studied (in the present case, strain rates of 15, 40, 60, 100 and 120 s^{-1} were selected) and determine at what values of time this strain rate is achieved

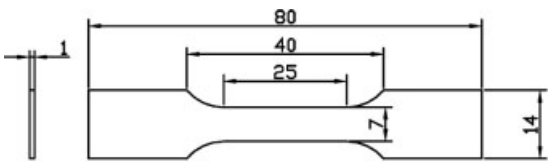

Figure 1. Geometry and dimensions of tensile impact samples.

Table 1. Constitutive coefficients for polypropylene

K (MPa s)	w	h	m	λ_{max}
49.55	35.36	0.855	0.041	1.49

for each impact velocity case. Then, for each of these values of time, the corresponding stress and strain pairs (σ_i, ε_i) are obtained from the $\varepsilon - t$ and the $\sigma - t$ curves simultaneously. For Eqn (2) to be valid a constant volume has been assumed and, therefore, the resulting $\sigma - \varepsilon$ curves at constant strain rate should be strictly called iso-nominal strain rate curves.

Falling weight impact tests

In falling weight impact tests, a hemispherical impactor dart of a specified mass is allowed to freely fall from a certain drop height (h) and penetrate a clamped disc-shaped test sample in the direction normal to its plane. At the initiation of contact, the velocity of the impactor is v_0. As impact takes place, a piezoelectric transducer in the impactor records the force exerted as a function of time. A force–displacement curve can be obtained by integrating the force with respect to time:

$$x = \frac{1}{m}\int_0^t \int_0^t F(t)\,\mathrm{d}t^2 + v_0 t \tag{3}$$

where m is the impactor mass, t is the test time, $F(t)$ is the measured force in the impactor and v_0 is the initial velocity of the impactor. In the present investigation, low-energy falling weight impact tests were carried out using a hemispherical impactor with a 12.7 diameter and a 2.244 kg mass. Disc-shaped test specimens of 80 mm in diameter and 4 mm in thickness were machined from injection-moulded plates with a nominal thickness of 4 mm. Various impact velocities were imposed by varying the drop height in an incremental manner: 25, 100, 200, 300, 400 and 500 mm. These values correspond to initial v_0 values of 0.7, 1.4, 1.98, 2.43, 2.8 and 3.13 m s^{-1}. The effect of friction between the impactor and the disc was assessed by analysing the influence of using a lubricating fluid on the impactor tip. For all impact velocities employed, the mass used ensured complete reduction of the impactor velocity, i.e. rebound of the impactor tip.

COMPUTATIONAL EFFORTS

Constitutive model and implementation

For the numerical simulations, the generalized von Mises flow rule was used as a three-dimensional framework to describe the instantaneous evolution of plastic strain with applied stress:

$$S_{ij} = \left(\frac{2\overline{\sigma}}{3\dot{\overline{\varepsilon}}}\right)\dot{\varepsilon}_{ij} \tag{4}$$

where S_{ij} and $\dot{\varepsilon}_{ij}$ are the deviatoric stress and strain rate tensors, respectively. Parameter $\dot{\overline{\varepsilon}}$ is the equivalent strain rate given by

$$\dot{\overline{\varepsilon}} = \sqrt{\frac{2}{3}\left(\dot{\varepsilon}_{ij}\cdot\dot{\varepsilon}_{ij}\right)} \tag{5}$$

Parameter $\overline{\sigma}$ is the equivalent stress given by

$$\overline{\sigma} = \sqrt{\frac{3}{2}\left(S_{ij}\cdot S_{ij}\right)} \tag{6}$$

In addition to the tensorial flow rule, the constitutive relationship between the invariant scalars $\overline{\sigma}$, $\overline{\varepsilon}$ and $\dot{\overline{\varepsilon}}$ needs to be specified. For this purpose, the G'Sell–Jonas viscoplastic phenomenological model, which expresses the stress evolution as a function of $\overline{\varepsilon}$ and $\dot{\overline{\varepsilon}}$ in a multiplicative formalism, was used:

$$\overline{\sigma} = K(T)\left(1 - \mathrm{e}^{-w\overline{\varepsilon}}\right)\mathrm{e}^{h\overline{\varepsilon}^2}\dot{\overline{\varepsilon}}^m \tag{7}$$

where K is the material consistency, $\left(1 - \mathrm{e}^{-w\overline{\varepsilon}}\right)$ describes the 'viscoelastic' response of the material (the beginning of the $\sigma - \varepsilon$ curve in a tensile test), $\mathrm{e}^{h\overline{\varepsilon}^2}$ represents the strain-hardening behaviour observed at large deformations, $\dot{\overline{\varepsilon}}^m$ expresses the strain rate dependence and $\overline{\varepsilon}$ is the cumulated strain defined by

$$\overline{\varepsilon} = \int_0^t \dot{\overline{\varepsilon}}\,\mathrm{d}t \tag{8}$$

The effect of temperature is incorporated in the $K(T)$ term through

$$K(T) = K_0 \exp\left(-\frac{a}{T}\right) \tag{9}$$

where K_0 is called the consistency pre-exponential factor and a is the thermal dependence coefficient.

The constitutive model was coded as a user-material subroutine (VUMAT) in the ABAQUS/Explicit finite element code. In the VUMAT, an algorithm of elastic prediction–plastic correction was applied to calculate the stress tensor at each material point where the first predicted stress tensor is based on generalized Hooke's law. At the end of each strain increment, the predicted stress tensor was corrected using the G'Sell–Jonas equation.

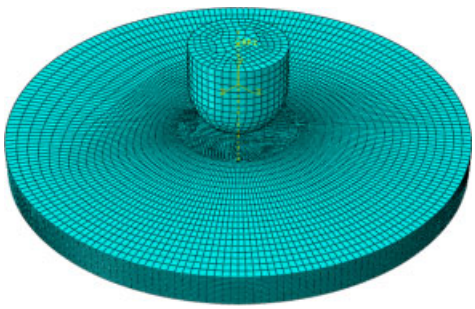

Figure 2. Mesh used for the simulation of the falling weight impact test.

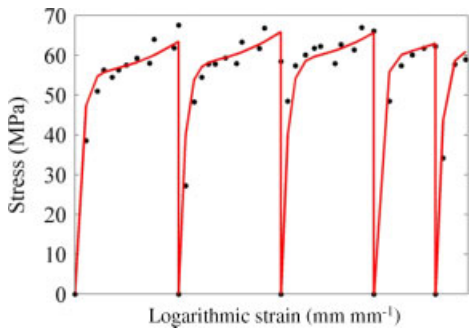

Figure 3. Experimental points (black dots) and simulated curves (solid lines) after the calibration of the G'Sell–Jonas constitutive model using inverse analysis. From left to right, the fives curves correspond to increasing strain rates of 15, 40, 60, 100 and 120 s^{-1}.

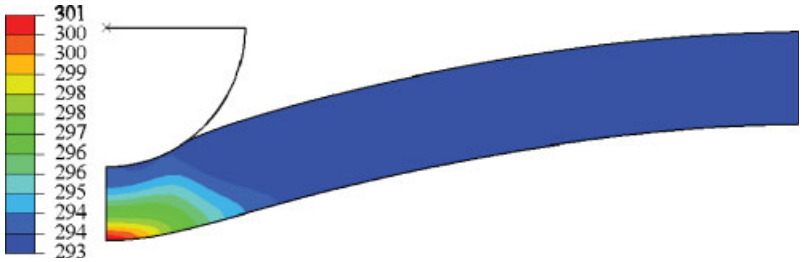

Figure 4. Cross-section showing temperature distribution (K) along the disc at maximum deflection during an impact test ($h = 500$ mm; $v_0 = 3.130$ m s^{-1}).

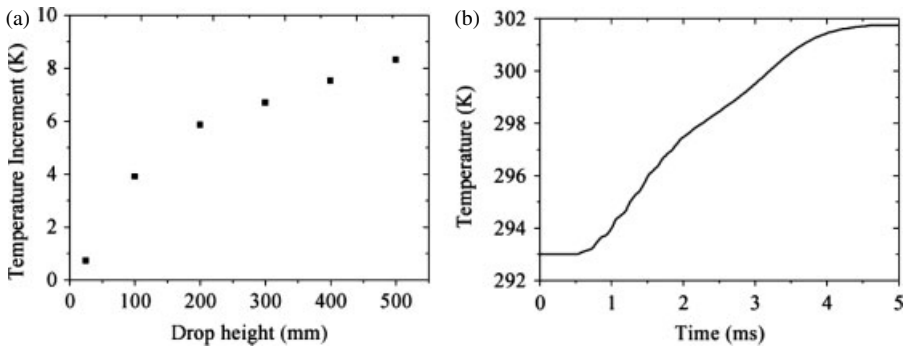

Figure 5. (a) Maximum temperature increment in the lower centre of a disc sample as a function of drop height. (b) Evolution of temperature in the lower centre of a disc sample ($h = 500$ mm; $v_0 = 3.130$ m s^{-1}).

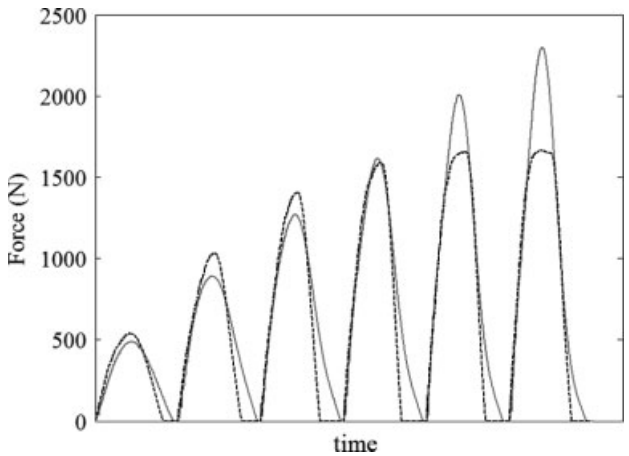

Figure 6. Experimental points (solid line) and simulated curves (dashed line) showing a comparison of the classical elastoplasticity model prediction for the multiaxial impact test. The curves are concatenated in increasing impact velocity order from left to right.

Inverse method: determination of constitutive parameters

To determine the constitutive coefficients for the G'Sell–Jonas equation, an inverse modelling analysis was adopted.[12] In this approach, a series of simulations of the isostrain rate tensile test are performed. For each simulation, the new constitutive parameters are determined iteratively by an optimization algorithm which seeks to minimize the value of a cost function Q with respect to the unknown constitutive parameters. The function Q quantifies the difference between the experimental curves and the simulated curves in a least squares formulation:

$$Q(\mathbf{x}) = \sum_{i=1}^{n} \left(\sigma_i^{\text{exp}} - \sigma_i^{\text{FEM}}(\mathbf{x})\right)^2 \qquad (10)$$

where vector $\mathbf{x}$ collects the unknown parameters, n is the number of experimental points, σ_i is the value of the tensile stress at each point and the superscripts 'exp' and 'FEM' denote experimental points and FEM simulated points, respectively. For the minimization of the cost function Q, the trust region algorithm was selected.

Prior to the application of the inverse analysis to the experimental data, a series of computational tests were carried out in order to check the validity of the method for this particular problem (i.e. to prove that the parameters obtained with this method are precise and unambiguous). The validation was performed as follows. First, 'experimental' curves were generated, by simulation of the tensile test, using constitutive parameters found in the literature.[5] Then, the goal was to reach these known values by running the inverse analysis optimization sequence starting with seed values, both one order of magnitude above and below the known parameters. It was found that when the analysis was carried out by calibrating simultaneously three different 'experimental' curves, each at a different strain rate, the method converged to the original parameters with a maximum relative error of 10^{-6}.

Following the validation stage, the inverse analysis was performed for the determination of the constitutive parameters from the experimental stress–strain curves. Isostrain rate curves at 15, 40, 65, 100 and 120 s^{-1} were used simultaneously as input data. The simulation of the isostrain rate tensile tests was modelled in ABAQUS/Explicit 6.10 using a rectangular geometry to represent the gauge section of the tensile tests. A total of 1300, C3D8R (8-node linear brick, reduced integration, hourglass control) three-dimensional elements were employed. Symmetry boundary conditions of zero displacement on the x-axis, z-axis and medial plane were defined in order to save computation time. For the calibration stage, all simulations were isothermal.

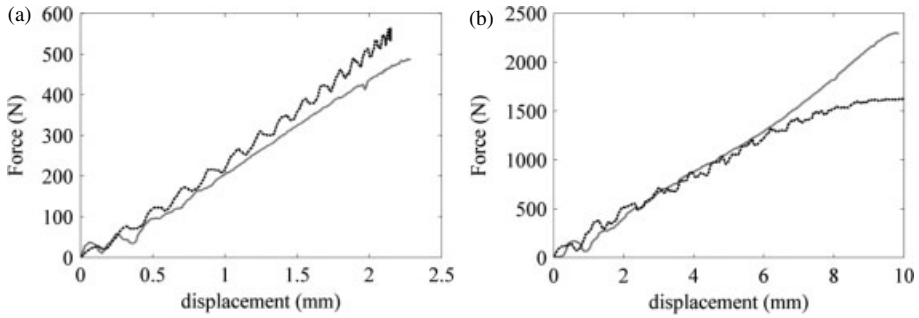

Figure 7. Experimental (solid line) and simulated (dashed line) force–displacement curves showing a comparison of the classical elastoplasticity model prediction for the multiaxial impact test: (a) $h = 25$ mm, $v_0 = 0.7$ m s^{-1}; (b) $h = 500$ mm, $v_0 = 3.13$ m s^{-1}.

Falling weight impact tests: finite element simulations

Once the constitutive parameters were determined at high strain rates from the tensile impact tests, the following step was to test the constitutive model under different loading conditions. For this purpose, the instrumented multiaxial impact test was used since it produces a force–displacement curve suitable for the comparison of simulated and experimental data. In order to study model prediction capabilities, simulations of the impact test were contrasted employing classical elastoplasticity constitutive behaviour on the one hand and the G'Sell–Jonas model on the other. In addition, the effect of thermomechanical coupling was studied by running simulations for all impact speeds on a coupled displacement–temperature step analysis in ABAQUS. The value for the thermal dependence coefficient a was taken from the literature[9] and the value of K_0 was obtained from the value of K determined previously (Table 1). A heat dissipation factor equal to 1 was employed. This means that all of the plastic deformation energy is turned into heat and incorporated into the heat transport equation (Eqn (9)), i.e. conservation of energy with the Fourier conduction law:

$$\rho C_p \frac{dT}{dt} = k\nabla^2 T + W \tag{11}$$

where T is the temperature, ρ the density, C_p the heat capacity, k the thermal conductivity and W the plastic heat generation rate. The values for the thermal properties of the polymer were taken from the literature.[8] This finite element model accounts for energy exchanges with the metallic clamps, the impactor tip and the surrounding air.

The falling weight test was simulated in ABAQUS/Explicit 6.10. Impact discs were modelled using C3D8R axisymmetric quadrilateral elements. Node density was biased towards the disc centre (Fig. 2). The impactor was modelled as a rigid surface. Contact definitions included frictionless tangential behaviour and a contact stiffness of 10^4 was defined for the normal behaviour in order to improve convergence rate. To model the clamps, zero-displacement boundary conditions were applied on the edge of the disc. Displacement and force outputs were requested on a reference point which was previously associated with the rigid body. Stress, strain and strain rate field outputs were requested for the entire piece. Impact velocities employed corresponded to those used in the experiments (0.7, 1.4, 1.98, 2.43, 2.8 and 3.13 m s^{-1}).

RESULTS AND DISCUSSION

Inverse analysis

Constitutive parameters for the G'Sell–Jonas equation were determined using the inverse analysis approach. The results

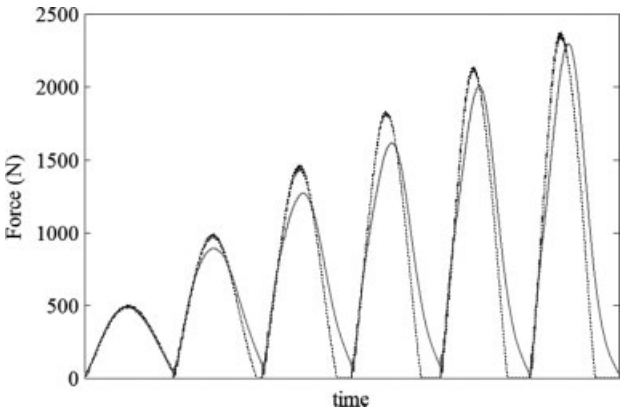

Figure 8. Experimental points (solid line) and simulated curves (dashed line) showing a comparison of the G'Sell–Jonas model prediction for the multiaxial impact test. The curves are concatenated in increasing impact velocity order from left to right.

are given in Table 1. Figure 3 shows the concatenation of experimental and simulated isostrain rate curves used for the inverse analysis. Five different curves were used simultaneously at different deformation rates (15, 40, 60, 100 and 120 s^{-1}) to ensure that the set of constitutive parameters is determined and unique. Otherwise, it is possible to fit each curve individually using different parameter sets. It is important to comment that fitting the curves analytically, i.e. without using FEM-assisted inverse analysis, would have given different solutions. This can be explained by the fact that the analytical approach does not take into account inertial effects and the initial transitory response at the beginning of the load case.

Impact tests: friction and thermomechanical coupling analysis

Falling weight curves with lubricated or non-lubricated impactor tip conditions were compared in order to study the effect of friction between the impactor tip and the test sample. The difference in the force–displacement curves for both cases is found to be negligible in the range of velocities used in this investigation.

The effect of plastic heat generation in the FEM simulations is also found to be undistinguishable since simulated curves for both cases, with thermomechanical coupling and with no thermal effects, overlap in all displacement ranges. Figure 4 shows the maximum increment in temperature, located in the centre of the disc and the opposite surface to the impact. In Fig. 5(a) it can be seen that, as expected, the heat dissipated (observed through increment of temperature) increases with drop height, .i.e. impact velocity.

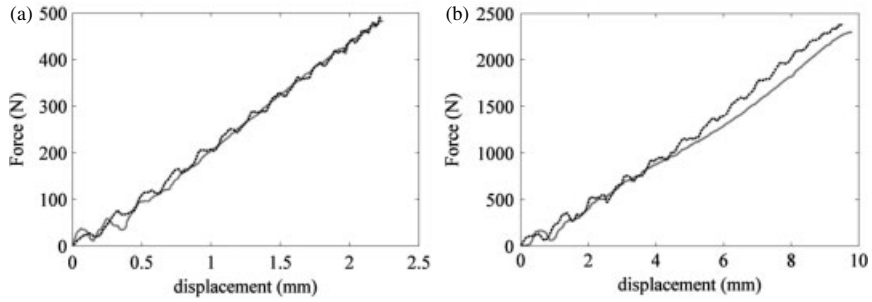

Figure 9. Experimental (solid line) and simulated (dashed line) force–displacement curves showing a comparison of the G'Sell–Jonas model prediction for the multiaxial impact test: (a) $h = 25$ mm, $v_0 = 0.7$ m s^{-1}; (b) $h = 500$ mm, $v_0 = 3.13$ m s^{-1}.

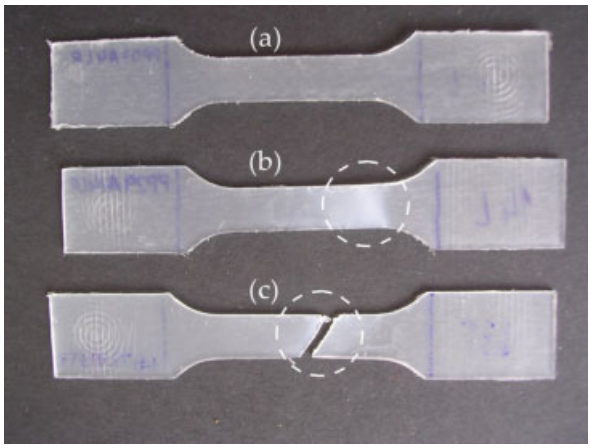

Figure 10. Tensile impact samples showing the three final stages of deformation before failure and the stress-whitening damage.

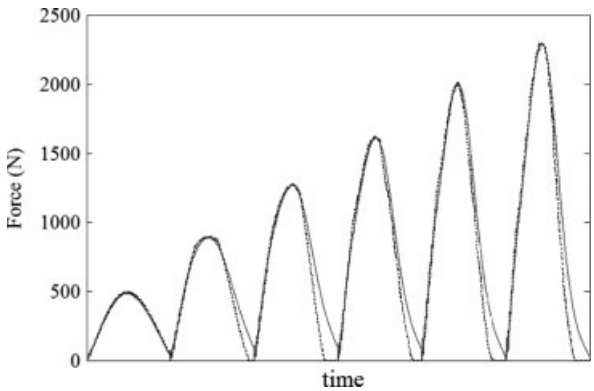

Figure 11. Experimental points (solid line) and simulated curves (dashed line) showing a comparison of the G'Sell–Jonas model prediction for the multiaxial impact test using a failure model. The curves are concatenated in increasing impact velocity order from left to right.

However, the maximum temperature rise ($\approx 8\,^{\circ}$C for the case of $v_0 = 3.13$ m s^{-1}, Fig. 5(b)) is not high enough to produce a significant change in the constitutive response, e.g. in the form of heat softening. This is expected since the impact energies employed are low and the thickness of impact samples is small enough to allow almost all heat to dissipate instantaneously. Moreover, the result is conservative since the G'Sell–Jonas equation is a viscoplastic law, in the sense that it considers all deformation as plastic and therefore introduces additional heat in the calculations.

Impact test simulation using classical elastoplasticity

In order to show the limitations of the classical models originally developed for metal plasticity, the falling weight impact test was first modelled with linear elastic behaviour followed by von Mises yielding and rate-independent hardening. Results are shown in Figs 6 and 7. In order to establish a more direct comparison, all the force–time curves belonging to the various impact velocities are concatenated in one single graphic. Force–displacement curves are shown up to the maximum experimental load. It can be observed that the initial slope, corresponding to the immediate viscoelastic response, is well reproduced with some minor deviations for the lower impact speed case (the first curve from the left). This can be directly explained by the non-rate-dependent elastic modulus used. More remarkable is the fact that at the lower impact speeds (drop heights of 25, 100 and 200 mm), the maximum force is overpredicted. Also, it is observed that up to $h = 300$ mm, yielding is not initiated in the simulations. On the other hand, starting from $h = 300$ mm the maximum force remains invariable and results in an underestimation of the actual experimental result. This fact can be explained by the use of a rate-independent yield stress, which is always reached approximately at the same impact force. In fact, the maximum force in the simulation is observed to correspond directly to the point when the outer layers in the central zone, where the von Mises stress is maximum, reach the yield stress. Beyond this point, in the simulations, the force begins to decrease, corresponding to the onset of the 'classical' plastic flow. However, experimental results show that the maximum force increases with impact speed.

Impact test simulation using G'Sell–Jonas model

The following step is to study the capability of the G'Sell–Jonas rate-dependent viscoplastic model. Figures 8 and 9 show simulated and experimental curves for the falling weight impact test. A much better fit can be observed: the initial slope is well reproduced at all impact speeds. Also, the increase of maximum force with impact speed can be predicted in all cases, i.e. yielding rate dependency is manifested. However, maximum impact load is overpredicted as impact speed increases. One possible explanation for this is the limitations in the model to accurately predict the multiaxial stress and strain states evolving in the material from purely uniaxial data. The impact test induces a biaxial stress state in most of the sample, with exception of the zone in contact with the impactor and the outer region in contact with the clamps. The G'Sell–Jonas model relates the tensile stress state with the strain tensor through the equivalent cumulated strain (Eqns (5) and (7)), a scalar obtained from the strain tensor. It is probable that this relationship requires to be modelled using more complex tensorial

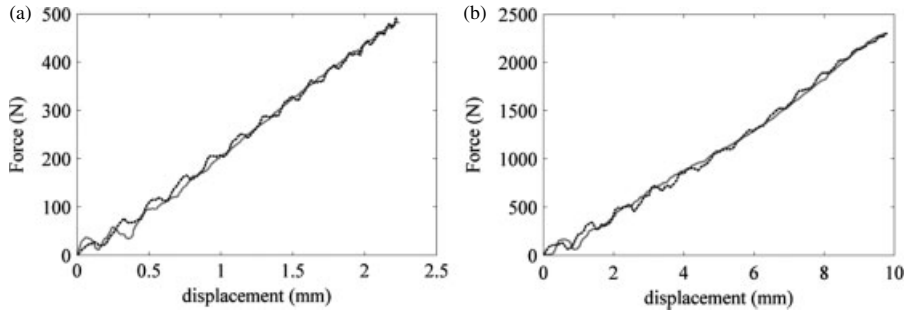

Figure 12. Experimental (solid line) and simulated (dashed line) force–displacement curves showing a comparison of the G'Sell–Jonas model prediction for the multiaxial impact test using a failure model: (a) $h = 25$ mm, $v_0 = 0.7$ m s^{-1}; (b) $h = 500$ mm, $v_0 = 3.13$ m s^{-1}.

functions. The stress whitening observed in both tensile and biaxial tests (Fig. 10) also contributes to this conclusion since it has been noted that crazing and whitening phenomena are the result of micro-voiding and opening up of cavitated regions.[13,14] This requires a careful characterization of the deformed chain structure into the strain tensor – and ultimately the stress tensor – that the G'Sell–Jonas model lacks.

However, one way of solving these limitations for this particular case is by modelling the stress whitening with a particular failure criterion which will work as a progressive damage mechanism in the simulations. There have been a number of attempts to establish a crazing criterion.[14,15] The most important assumption is that, since it is a cavitation phenomenon, it should take place at a critical strain.[16] In this investigation, the chain stretch failure is used:

$$\lambda_{\text{chain}} = \sqrt{\frac{1}{3}\left(e^{2\varepsilon_1} + e^{2\varepsilon_2} + e^{2\varepsilon_3}\right)} \tag{12}$$

where ε_i are the principal strains. This failure model was selected as an oversimplification; its most important features are that it can be readily implemented in the VUMAT and it is dependent on an adequate critical strain measure. Failure behaviour based on the maximum chain stretch was imposed using the element deletion option in ABAQUS. This means that at the end of each iteration, VUMAT calculates the λ_{chain} value at every integration point. If the λ_{chain} value exceeds a critical chain stretch value, λ_{max}, then the element associated with this point is removed and exerts no resulting stress.

The chain stretch criterion was originally developed[17] to reproduce overall failure behaviour of ultrahigh-molecular-weight polyethylene, another semicrystalline polymer, and was shown to have a much lower variability between various tests and better overall agreement with both uniaxial and multiaxial experimental failure data than any other failure models. In this investigation, the critical chain stretch value was determined by iterative inverse analysis from the impact curves.

Figures 11 and 12 show simulated curves taking into account failure behaviour. In all cases, predicted and experimental curves up to the maximum force are obtained. This is expected since it is enforced when calibrating the critical value for the failure criterion. On the other hand, the maximum strain rate attained calculated in the simulations is equal to 1.1×10^3 s^{-1} which is an order of magnitude higher than the maximum strain rate (120 s^{-1}) used for the determination of the constitutive parameters, showing that the extrapolation to strain rates ten times higher can be considered valid.

CONCLUSIONS

Constitutive parameters for the G'Sell–Jonas constitutive model were obtained from experimental tensile impact tests using the inverse analysis methodology. Prediction capability of this model was studied by comparison of FEM simulated and experimental curves for the falling weight impact test. The model described accurately the initial response; however, it overpredicted the maximum load. This inaccuracy was related to the inability of the constitutive model to extrapolate uniaxial stress–strain states to more complex multiaxial states. A forthcoming work will evaluate the predictability of more complex tri-dimensional constitutive models. To improve the model, the maximum chain stretch failure criterion was incorporated which models the material damage that was observed in the form of stress whitening. It was shown that material parameters deduced from tensile impact tests can be successfully transferred to a different loading scenario, i.e. multiaxial load, using the G'Sell–Jonas equation together with the chain stretch failure criterion.

REFERENCES

1 Duan Y, Saigal A, Greif R and Zimmerman MA, *Polym Eng Sci* **43**:112–124 (2003).
2 Mulliken AD and Boyce MC, *Int J Solids Struct* **43**:1331–1356 (2006).
3 Aretxabaleta L, Aurrekoetxea J, Urrutibeascoa I and Sanchez-Soto M, *Polym Test* **24**:145–151 (2005).
4 Aretxabaleta L, Aurrekoetxea J, Castillo G and Mateos M, *Polym Test* **27**:84–92 (2007).
5 G'Sell C and Jonas J, *J Mater Sci* **14**:583–592 (1979).
6 Duffo P, G'Sell C, Dahoun A, Monasse B and Haudin JM, *J Mater Sci* **30**:701–711 (1995).
7 Duan Y, Saigal A, Greif R and Zimmerman MA, *Polym Eng Sci* **41**:1322–1328 (2001).
8 Billon N, Schang O, Muracciole JM and Fernagut F, *Polym Eng Sci* **36**:541–550 (1996).
9 Viana JC, Cunha AM and Billon N, *Polym Eng Sci* **97**:337–346 (2007).
10 Boyce MC, Parks DM and Argon AS, *Mech Mater* **7**:15–33 (1988).
11 Arruda E, Boyce M and Jayachandran R, *Mech Mater* **19**:193–212 (1995).
12 Pettarin V, Frontini P and Eliçabe G, Inverse method for the analysis of instrumented impact tests of polymers, in *Fracture of Polymers, Composites and Adhesives*, ed. by Blackman BRK, Pavan A and Williams JG. Elsevier Science, London, pp. 265–278 (2003).
13 Argon AS, *Polymer* **52**:2319–2327 (2011).
14 Liu Y, Kennard C, Truss RW and Calos NJ, *Polymer* **38**:2797–2805 (1997).
15 Rottler J, *J Phys Condens Matter* **21**:463101 (2009).
16 Young RJ and Lovell PA, *Introduction to Polymers*, 3rd edition. CRC Press, Boca Raton, FL, pp. 531–555 (2011).
17 Bergström JS, Rimnac CM and Kurtz SM, *J Orthop Res* **23**:367–375 (2004).

